Ultrafast dynamics of low-energy electron attachment via a non-valence correlation-bound state

*Joshua P. Rogers, Cate S. Anstöter and Jan R. R. Verlet**

Department of Chemistry, Durham University, Durham DH1 3LE, United Kingdom.

*j.r.r.verlet@durham.ac.uk

Abstract

The primary electron attachment process in electron driven chemistry represents one of the most fundamental chemical transformations with wide-ranging importance in science and technology. However, the mechanistic detail of the seemingly simple reaction of an electron and a neutral to form an anion remains poorly understood, particularly at very low electron energies. Here, time-resolved photoelectron imaging was used to probe the electron attachment process to a non-polar molecule using time-resolved methods. An initially populated diffuse non-valence state of the anion that is bound by correlation forces evolves coherently in ~30 fs into a valence state of the anion. The extreme efficiency with which the correlation-bound state serves as a doorway state for low-energy electron attachment explains a number of electron driven processes such as anion formation in the interstellar medium and electron attachment to fullerenes.

Introduction

The attachment of an electron to a neutral molecule represents one of the most fundamental chemical transformations with importance in many branches of science and technology. It is the primary process in electron driven chemistry and a key reaction in diverse fields such as radiation chemistry; plasma science, medicine and technology; astro-chemistry and physics; atmospheric chemistry; and mass-spectrometry.[1,2] Because of its ubiquity, electron attachment has been actively studied for many decades. However, despite this vast body of work, key mechanistic and dynamical details of the process remain poorly understood, especially at very low electron energies.

In general, electron attachment is accepted to proceed via excited states that are embedded in the continuum (resonances) of the respective anion, and it is the fate of these resonances that dictates the outcome of the reaction.[1,3] At very low energy, only electrons with no orbital angular moment ($l = 0$) can be captured and require molecular orbitals of the anion with the correct symmetry to be available.[1,2] However, it has also been observed that neutral molecules with large dipole moments have an enhanced attachment cross section near threshold.[4] It is believed that diffuse non-valence electronic states of the anion may act as doorway states to forming the parent anion[5] and this is supported by the observation of resonances in electron attachment and anion photodetachment experiments.[2,6–8] The prime candidate for such doorway states are dipole bound states that arise from the long-range interaction between a permanent dipole of a molecule and the excess electron.[9,10] However, molecules with no permanent dipole, such as C_{60}, also display large attachment cross sections.[11,12] Theoretical work has shown that correlation forces are also important in non-valence states and can even dominate electron binding leading to a so-called non-valence correlation-bound state (CBS),[10,13–18] which was very

recently observed spectroscopically.[19] Indeed, calculations showed that correlation forces alone can be sufficient to bind an electron.[20–25] Hence, it has also been suggested that the presence of a non-valence CBS may facilitate electron attachment.[24]

A most striking example of a non-valence CBS is in the anion of hexafluorobenzene, $C_6F_6^-$, where it is predicted to be bound by >100 meV.[24] Indeed, two-photon photoemission and STM experiments of C_6F_6 on Cu(111) surfaces have suggested that diffuse anions states are formed during the electron capture process.[26,27] As the electron in the CBS is associated with the neutral core, the potential energy surface of the CBS is similar to that of the neutral ground electronic state. For C_6F_6, this is a planar geometry akin to benzene. However, the lowest energy structure of $C_6F_6^-$ is a valence-bound anion in which the anion adopts a buckled geometry.[24,28,29] Calculations have suggested that the non-valence CBS can undergo a barrierless conversion to form the valence-bound anion.[24] Because of the large difference in geometries between the valence and non-valence anions of C_6F_6, this molecule represents an ideal model system to probe the mechanistic details of electron attachment.[28,29] Moreover, C_6F_6 may be viewed as being representative of a number of aromatic systems. For example, several molecules such as C_{60}^- and large polycyclic aromatic hydrocarbon anion have been calculated to support a CBS.[20,22,23,25] Here, we present compelling evidence for the formation of a non-valence CBS of $C_6F_6^-$ followed by extremely efficient evolution of the CBS of into the valence-bound anion, preserving coherence into the vibrational modes of the valence-bound anion.

Results and Analysis

To mimic the electron impact process, we used photoexcitation of iodide in the $I^-\cdot C_6F_6$ cluster as an electron source. The use of photoexcitation of an anion clustered to a neutral

molecule has been developed and exploited as a sensitive probe of a range of charge-induced processes including solvation, electron driven chemistry and the formation of dipole-bound states.[8,30] It has also been extended to the time-domain enabling electron impact dynamics to be probed in real-time.[31] In our experiments, cold weakly-bound clusters of $I^-\cdot C_6F_6$ were generated in a pulsed supersonic expansion, mass-selected, and then irradiated by pulses from a tuneable nanosecond laser at the centre of a velocity-map imaging photoelectron spectrometer.[32] The measured electron kinetic energy (eKE) represents the difference in energy between the anion and neutral complexes at the geometry of the anion.

Fig. 1a shows a false-colour map of the photoelectron spectra as a function of photon energy, *hv*. Each photoelectron spectrum has been normalised to its total electron yield. There are two prominent photoelectron features, each with eKE that increases by an amount commensurate with increasing *hv* (features (i) and (ii) in Fig. 1a). The energy gap between these two narrow photoelectron peaks is 0.94 eV and can be assigned to direct detachment from $I^-\cdot C_6F_6$ to the neutral $I[^2P_{3/2}]\cdot C_6F_6$ and $I[^2P_{1/2}]\cdot C_6F_6$ species. The onset of the $I[^2P_{3/2}]\cdot C_6F_6$ indicates that the adiabatic detachment energy of $I^-\cdot C_6F_6$ is 3.49 eV, which is 0.43 eV higher that the electron affinity of I (3.059 eV) and primarily corresponds to the cluster cohesion energy. In addition to the direct detachment peaks, photoelectron signals below the onset of the $I[^2P_{3/2}]\cdot C_6F_6 + e^-$ channel are observed. The peak with adiabatic binding energy of 3.06 eV, indicated as feature (iii) in Fig. 1a, is consistent with photodetachment of unclustered I^-. A photoelectron spectrum at hv = 3.40 eV (Fig. 1b) clearly shows this peak as well as a weak and broad feature at higher eKE. The high-eKE peak has the appearance of the photoelectron spectrum of $C_6F_6^-$ but shifted to higher binding energy by ~0.3 eV. This peak may be assigned to photodetachment from $I\cdot C_6F_6^-$.

The photodetachment of I^- and $I{\cdot}C_6F_6^-$ below the adiabatic detachment energy of $I^-{\cdot}C_6F_6$ indicates that an excited state of $I^-{\cdot}C_6F_6$ can be accessed, which subsequently forms $I{\cdot}C_6F_6^-$ and then may dissociate to form $I^- + C_6F_6$ within the duration of the ~5 ns laser pulse. According to Fig. 1a, these dynamics are observed over a spectral range of at least 0.4 eV. Finally, around $h\nu$ ~ 4.2 eV, a feature ((iv) in Fig. 1a) can be seen that peaks near eKE = 0 eV, indicative of a similarly broad absorption band below the onset of the $I[^2P_{1/2}]{\cdot}C_6F_6 + e^-$ channel. A representative photoelectron spectrum is shown in Fig. 1c, which additionally shows features that can be assigned to $I[^2P_{3/2}]{\cdot}C_6F_6 + e^-$ and $I + e^-$ direct detachment channels.

To probe the dynamics of the excited state, time-resolved photoelectron imaging was used, as this method is sensitive to both electronic structure evolution and nuclear dynamics and can in principle track the dynamics along the entire reaction coordinate.[33] A femtosecond pump pulse at 3.10 eV (400 nm) excited $I^-{\cdot}C_6F_6$ in the range where I^- signal was observed (Fig. 1a) and therefore accesses the excited state of $I^-{\cdot}C_6F_6$. A second femtosecond probe pulse at 1.55 eV (800 nm) tracked the subsequent dynamics. The optical delay between the pump and probe pulses defines the time axis, *t*. The measured photoelectron spectra reflect those of the temporally evolving photoexcited anion at the instant it was probed.

Fig. 2a shows the observed dynamics as a false colour plot. At $t = 0$, denoted by the vertical dashed line, a bright and spectrally narrow photoelectron feature can be observed at eKE = 1.10 eV. A high-quality photoelectron spectrum taken around $t = 0$ is shown in Fig. S1. A second less-intense feature with similar dynamics appears at eKE = 0.15 eV. The high eKE feature evolves into a much weaker peak that rapidly shifts towards lower eKE. Around $t = 180$ fs, much of the intensity has disappeared but subsequently recovers after 300 fs and oscillates to

a constant signal level at long times (t > 1.5 ps). At eKE < 0.1 eV, a feature increases in intensity over the first ~1 ps.

Photoelectron imaging also provides information about the angle, θ, of the emitted electron velocity vector relative to the laser polarisation axes. The photoelectron angular distribution is quantified by the anisotropy parameters, β_2 (and β_4 for a 2-photon process), which lies between the limiting cases of $\beta_2 = +2$ ($\cos^2\theta$) and $\beta_2 = -1$ ($\sin^2\theta$). In Fig. 2b, β_2 is presented as a function of t and eKE, where a 9-point moving average was applied along the eKE axis to improve the signal-to-noise. The corresponding β_4 plot is presented in Fig. S2. The peak at eKE = 1.10 eV and t = 0 has $\beta_2 = +1.0$, corresponding to emission predominantly parallel to the polarisation axes. Signal in the 0.2 < eKE < 1.0 spectral range for t > 0 has a similar but more pronounced distribution with $\beta_2 \sim +2$. Finally, for eKE < 0.1, the signal is mostly isotropic.

To analyse the dynamics in more detail, we have integrated the time-resolved photoelectron signal over representative spectral ranges as indicated by the coloured brackets in Fig. 2a. The results of this are shown in Fig. 2c. The dynamics of the high eKE feature (integration window 1.0 < eKE < 1.2 eV) has a Gaussian profile that essentially reproduces the cross-correlation between the pump and probe pulses; a fit to the data is included in Fig. 2c. The photoelectron signal in integration window 0.25 < eKE < 0.60 eV clearly shows the oscillatory nature of the feature apparent from Fig. 2a. A fast Fourier transform of the data yields a frequency of 121±2 cm^{-1}. These data were also fitted to a decaying cosine function as shown in Fig. 2c. The lifetimes of the decays are on the order of 400 fs, but vary with spectral integration range. A phase of –0.6 rad was required for the fit. Finally, Fig. 2c also includes the integrated signal at eKE < 0.1 eV. Signal in this range increases in a step-like fashion that is nearly out-of-phase with the feature in the 0.25 < eKE < 0.60 eV window.

Electronic structure calculations were used to characterise $I^-{\cdot}C_6F_6$ and to gain qualitative insight into the excited state accessed by photoexcitation at 3.10 eV. The minimum energy structure of $I^-{\cdot}C_6F_6$ shows that I^- is located above the planar C_6F_6 and that the excess electron resides on I^- (see Fig. 3), in agreement with the narrow direct detachment peak from the cluster seen in Fig. 1a. The molecular orbital associated with the initially photoexcited state, $[I{\cdot}C_6F_6^-]^*$, is diffuse and predominantly of s-character and involves a charge transfer from I^- onto the C_6F_6 ring (see Fig. 3). The $[I{\cdot}C_6F_6^-]^*$ orbital is very similar in appearance to the CBS calculated by Voora and Jordan for $C_6F_6^-$ using higher level of theory.[24]

Discussion

Immediately following photoexcitation, $t = 0$, the photoelectron spectrum corresponds to the spectrum of the initially excited state, which shows an intense peak at eKE = 1.10 eV. A much weaker peak (eKE = 0.15 eV) is offset by the spin-orbit splitting of iodine and suggest that detachment from the initially excited state is predominantly associated with the $^2P_{3/2}$ final state. The angular distribution associated with the peak at eKE = 1.10 eV is anisotropic ($\beta_2 = +1.0$) with photoelectrons being emitted predominantly parallel to the polarisation axis of the probe (see inset in Fig. 3). This is in stark contrast to the anisotropy of photoelectrons with the same eKE generated by a single-photon excitation (*i.e.* $h\nu = 4.65$ eV) which are emitted predominantly perpendicular to the polarisation axis ($\beta_2 = -0.75$). The initial $\beta_2 = +1.0$ is consistent with detachment from a non-valence s-like orbital and similar to that recently measured for a non-valence CBS,[19] while the negative β_2 is expected for detachment from the I^- 5p-electrons at this eKE. In addition, the relative intensity of this peak points to a large photodetachment cross section. To a first approximation, the cross section for photoemission may be expected to be very large when the de Broglie wavelength (λ) of the outgoing electron approaches the spatial extent

of the orbital from which the electron is removed.[34] At eKE = 1.1 eV, λ = 12 Å, which is close to the spatial extent of the CBS calculated by Voora and Jordan (~ 10 Å).[24] Furthermore, photoelectron spectra of dipole-bound anions have been observed to have vibrational structure which arises not only from differences in anion and neutral surfaces, but also from vibrational modes of the neutral that are strongly coupled to the non-valence state (*i.e.* IR active modes for dipole bound states).[34] Vibrational structure is also observed here (Fig. S1), with a peak red-shifted by ~1450 cm^{-1}. For a non-valence CBS, both Raman and IR modes could modulate the orbital binding and the measured frequency is close to the 1490 cm^{-1} Raman active a_{1g} mode or the very bright IR active 1530 cm^{-1} e_{1u} mode of planar (D_{6h}) C_6F_6.[35] Taken together, these observations are consistent with the formation of a non-valence state of $C_6F_6^-$ immediately following excitation of $I^-\cdot C_6F_6$ at $h\nu$ = 3.10 eV.

The binding energy of the intermediate state is ~0.4 eV. This is different from the 140 meV calculated by Voora and Jordan,[24] and a recent calculation suggests a similar electron binding energy of the CBS with the neutral iodine present.[36] Nevertheless, Fig. 1a clearly shows that the excited state can be accessed over a broad (~0.4 eV) spectral range. A similarly wide absorption range has previously been noted for excitation to a non-valence dipole bound state in $I^-\cdot$Pyrrole clusters.[37]

The narrow peak at eKE = 1.10 eV decays within the time-resolution of the experiment (<40 fs) and evolves into a peak at lower eKE, suggesting that the electron binding energy rapidly increases. Indeed, close inspection of the time-resolved photoelectron spectra over the first 100 fs reveals that the average eKE is rapidly shifting towards lower values. This evolution suggests a rapid increase in the energy of the final neutral state. Additionally, Fig. 2a shows a very rapid decrease in intensity as eKE decreases. The rapid reduction of signal suggests that the

spatial extent of the non-valence orbital decreases very rapidly.[34,38] Finally, Fig. 2b shows a rapid change in photoelectron anisotropy from $\beta_2 = +1.0$ for the narrow peak to $\beta_2 \sim +2$ for the broad feature. The changing photoelectron anisotropy points to changing electronic character. Photodetachment from the valence state of isolated $C_6F_6^-$ leads to a photoelectron angular distribution with $\beta_2 = +2$ (see Fig. S3) and therefore suggests that the valence state of $C_6F_6^-$ is formed. The observations are consistent with a non-valence CBS evolving into the valence state of $C_6F_6^-$, as predicted by Voora and Jordan.[24] This is shown schematically in Fig. 3. The relevant nuclear coordinate for this evolution is the buckling angle that connects the planar geometry of C_6F_6 to the buckled geometry of the lowest energy $C_6F_6^-$ conformation (see Fig. 3).[24] This change is associated with a steep increase in the electron binding energy. At the minimum energy geometry of $C_6F_6^-$, the vertical and adiabatic binding energy are 1.45 and ~0.5 eV, respectively,[39–41] excluding the additional binding that arises from the cohesion energy of $C_6F_6^-$ to I. Hence, for a probe photon with $h\nu = 1.55$ eV, we anticipate a reduced photoelectron yield at the minimum buckled geometry of $I{\cdot}C_6F_6^-$. The time-resolved photoelectron spectra in Fig. 2a capture these dynamics. In the $0.25 < eKE < 0.60$ eV spectral range, photoelectron signal is observed to oscillate in intensity with a 275 fs period. A large photoelectron signal signifies a small energy gap between anion and neutral states, which corresponds to a small buckle angle (*i.e.* closer to planar); a weak signal signifies that $I{\cdot}C_6F_6^-$ is at the other turning point where the buckle angle is maximal. We calculated the frequency of this buckling mode (shown in Fig. 3) to be 120 cm^{-1}, in close agreement with observations. The decay of the oscillation amplitude arises from a dephasing of the vibrational wavepacket and/or internal vibrational relaxation of the buckling mode into other modes of the cluster.

The rising feature at eKE < 0.1 eV also tracks the dynamics. The phase shift with respect to the direct detachment from $I \cdot C_6F_6^-$ suggests that this feature arises from photodetachment by the probe when the $C_6F_6^-$ is strongly buckled. We speculate that the probe passes through resonance with an electronic transition in $C_6F_6^-$, which eventually autodetaches to produce low eKE electrons. This interpretation is consistent with the isotropic angular distribution seen for electrons with eKE < 0.1 eV (Fig. 2b) and with previous photoelectron imaging studies.[37,42,43]

From the data, the time taken from the initial excitation to the minimum energy structure can be estimated to be ~100 fs. Based on the observed period of a full oscillation (275 fs), the motion from the planar to minimum energy structure is one quarter of the period (~70 fs). Hence, it appears that the initial evolution from the non-valence CBS into the valence orbital has a ~30 fs timescale associated with it. This is consistent with the phase shift (–0.6 rad) required to fit the data in Fig. 2c. Based on the calculations from Voora and Jordan, this 30 fs would therefore correspond to the change in electronic character from the non-valence to valence state of $C_6F_6^-$.

Whilst the data presented is consistent with the intermediate being the non-valence CBS predicted by Voora and Jordan,[24] the discrepancy in the measured and computed binding energy warrants caution. An alternative mechanism is direct injection into the valence orbital of $C_6F_6^-$. Because the valence state of $C_6F_6^-$ has different electronic character to the bent geometry, a change in photoelectron angular distribution may also be expected in this case. However, such a process would lead to a broad electron distribution and is not expected to show a delay in its formation, as observed here.

Most striking is the apparent coherence of the evolution from the CBS to the valence state, which further confirms that the wavepacket trajectory is very well-defined and few other

modes of the molecule (or cluster) are excited during the electron localisation. From an electron attachment perspective, these observations demonstrate that a non-valence CBS can act as an exceedingly efficient doorway state to the formation of an anion. The origin of the coherence is not yet clear. The absorption spectrum may contain vibrational structure of the $C_6F_6^-$ valence state. Vibrational Feshbach resonances have been seen in very low energy electron scattering experiments[6,44] and in intra-cluster photoexcitation spectra,[8,45] suggesting this may be the case. Excitation with the femtosecond pump (>400 cm^{-1} laser bandwidth) would create a coherent vibrational wavepacket and lead to the coherence observed in the valence anion. A linear action spectrum of the charge-transfer state accessed in the current experiment will provide insight into this.

A second detachment channel is evident in Fig. 1a. This occurs at around $h\nu \sim 4.2$ eV, below the $I[^2P_{1/2}]\cdot C_6F_6 + e^-$ channel and consists of a photoelectron feature peaking near eKE = 0 eV. This feature appears alongside the ejection of I^- from the cluster (Fig. 1c), which again points to the presence of an excited state. However, as the total energy is above the adiabatic energy of the cluster, the low eKE electrons are the product of autodetachment. Such excited state resonances have previously been observed and studied in detail using photoelectron imaging.[42,43] The timescale of this autodetachment was not probed here, but appears to be relatively slow given that back transfer to produce I^- is able to compete (Fig. 1c).

The observation of an exceedingly efficient mechanism for low-energy electron attachment in non-polar molecules indicates that non-valence CBS orbitals provide a doorway to forming stable anions and explains, for example, how polycyclic aromatic hydrocarbon and fullerene anions may be formed in the interstellar medium. More generally, our results provide a

detailed mechanistic understanding of one of the most fundamental chemical reactions, and provide an experimental window into the low-energy electron driven chemistry.

Methods and Materials

Clusters were generated by passing a mix of CF_3I (0.5 %) in 3.0 bar of Ar over a sample of liquid C_6F_6 and expanding this into vacuum through a pulsed valve to produce a molecular beam. The expansion was crossed with an electron beam (300 eV) to produce various clusters containing I and C_6F_6, including $I^-{\cdot}C_6F_6$. The molecular beam was injected orthogonally into a Wiley-McLaren time-of-flight mass spectrometer to allow mass-separation. The focus of the mass-spectrometer coincided with centre of a velocity-map imaging photoelectron spectrometer where the mass-selected $I^-{\cdot}C_6F_6$ ion packet was intersected with light pulses either from a nanosecond Nd:YAG pumped OPO or derived from a Ti:Sapphire amplified femtosecond laser system. Pump pulses at 3.10 eV (25 μJ) were generated by second harmonic generation in a thin BBO crystal and combined collinearly with probe pulses 1.55 eV (150 μJ) and focussed gently into the interaction region. Photoelectron images were detected on a position sensitive detector (dual microchannel plate with phosphor screen) and the electron positions recorded using a CCD. Crushed raw images were reconstructed using the polar onion peeling algorithm[46] and all photoelectron spectra were calibrated to the known spectrum of O_2^-. The spectral resolution $\Delta eKE/eKE = 2.6$ % and the temporal cross correlation is 70 fs, offering an ultimate time-resolution of <40 fs.

Density functional theory (DFT) calculations were performed on bare $C_6F_6^-$ using the QChem 4.4 package[47] and the CAM-B3LYP functional[48] with the aug-cc-pVDZ Dunning basis

set,[49] shown to perform well on anionic species.[50–52] Calculations on the $I^{-}\cdot C_6F_6$ cluster used the same level of theory, with the addition of the pseudopotential aug-cc-pVDZ basis set on the heavy I atom.[53] The geometries of ground state species were optimized and verified to be the geometric minima by vibrational frequency analysis. The calculated energetics have been corrected for zero-point energy. Additional time-dependent DFT calculations employed to characterise the excited state of the $I^{-}\cdot C_6F_6$ cluster and provide energetics used the same level of theory as ground state calculations.

Acknowledgements

We thank James N. Bull for his valuable contribution in building the experiment that enabled this work. This work was funded by the European Research Council under Starting Grant 306536.

Author Contributions

JRRV conceived the experiments. JPR conducted the experiments and CSA the calculations. JPR, CSA and JRRV analysed the data and discussed the results. JRRV wrote the manuscript with contributions from JPR and CSA.

Competing Financial Interests

The authors declare no competing financial interests.

References and Notes

1. *Electron–Molecule Interactions and their Applications*. (Academic Press, 1984). doi:10.1016/B978-0-12-174401-4.50001-8
2. Hotop, H., Ruf, M.-W., Allan, M. & Fabrikant, I. I. Resonance and Threshold Phenomena in Low-Energy Electron Collisions with Molecules and Clusters. *Adv. At. Mol. Opt. Phys.* **49,** 85–216 (2003).
3. Schulz, G. J. Resonances in Electron Impact on Diatomic Molecules. *Rev. Mod. Phys.* **45,** 423–486 (1973).
4. Desfrançois, C., Abdoul-Carime, H., Khelifa, N. & Schermann, J. P. From $1/r$ to $1/r^2$ Potentials: Electron Exchange between Rydberg Atoms and Polar Molecules. *Phys. Rev. Lett.* **73,** 2436–2439 (1994).
5. Sommerfeld, T. Dipole-bound states as doorways in (dissociative) electron attachment. *J. Phys. Conf. Ser.* **4,** 245 (2005).
6. Schramm, A. *et al.* Vibrational resonance and threshold effects in inelastic electron collisions with methyl iodide molecules. *J. Phys. B At. Mol. Opt. Phys.* **32,** 2153 (1999).
7. Mead, R. D., Lykke, K. R., Lineberger, W. C., Marks, J. & Brauman, J. I. Spectroscopy and dynamics of the dipole-bound state of acetaldehyde enolate. *J. Chem. Phys.* **81,** 4883–4892 (1984).
8. Dessent, C. E. H., Kim, J. & Johnson, M. A. Spectroscopic observation of vibrational Feshbach resonances in near-threshold photoexcitation of $X^- \cdot CH_3NO_2$ ($X^- = I^-$ and Br^-). *Faraday Discuss.* **115,** 395–406 (2000).
9. Jordan, K. D. & Wang, and F. Theory of Dipole-Bound Anions. *Annu. Rev. Phys. Chem.* **54,** 367–396 (2003).
10. Simons, J. Molecular Anions. *J. Phys. Chem. A* **112,** 6401–6511 (2008).
11. Weber, J. M., Ruf, M.-W. & Hotop, H. Rydberg electron transfer to C_{60} and C_{70}. *Z. Für Phys. At. Mol. Clust.* **37,** 351–357 (1996).

12. Finch, C. D., Popple, R. A., Nordlander, P. & Dunning, F. B. Formation of long-lived C_{60}^- ions in Rydberg atom-C_{60} collisions. *Chem. Phys. Lett.* **244,** 345–349 (1995).
13. Sommerfeld, T., Bhattarai, B., Vysotskiy, V. P. & Cederbaum, L. S. Correlation-bound anions of NaCl clusters. *J. Chem. Phys.* **133,** 114301 (2010).
14. Simons, J. & Gutowski, M. Double-Rydberg molecular anions. *Chem. Rev.* **91,** 669–677 (1991).
15. Sommerfeld, T., Dreux, K. M. & Joshi, R. Excess Electrons Bound to Molecular Systems with a Vanishing Dipole but Large Molecular Quadrupole. *J. Phys. Chem. A* **118,** 7320–7329 (2014).
16. Sommerfeld, T. Excess Electrons Bound to Small Ammonia Clusters. *J. Phys. Chem. A* **112,** 11817–11823 (2008).
17. Sommerfeld, T. Multipole-bound states of succinonitrile and other dicarbonitriles. *J. Chem. Phys.* **121,** 4097–4104 (2004).
18. T. Snodgrass, J., V. Coe, J., B. Freidhoff, C., M. McHugh, K. & H. Bowen, K. Photodetachment spectroscopy of cluster anions. Photoelectron spectroscopy of $H^-(NH_3)_1$, $H^-(NH_3)_2$ and the tetrahedral isomer of NH^-_4. *Faraday Discuss. Chem. Soc.* **86,** 241–256 (1988).
19. Bull, J. N. & Verlet, J. R. R. Observation and ultrafast dynamics of a nonvalence correlation-bound state of an anion. *Sci. Adv.* **3,** e1603106 (2017).
20. Klaiman, S., Gromov, E. V. & Cederbaum, L. S. All for one and one for all: accommodating an extra electron in C_{60}. *Phys. Chem. Chem. Phys.* **16,** 13287–13293 (2014).
21. Bezchastnov, V. G., Vysotskiy, V. P. & Cederbaum, L. S. Anions of Xenon Clusters Bound by Long-Range Electron Correlations. *Phys. Rev. Lett.* **107,** 133401 (2011).
22. Voora, V. K., Cederbaum, L. S. & Jordan, K. D. Existence of a Correlation Bound s-Type Anion State of C_{60}. *J. Phys. Chem. Lett.* **4,** 849–853 (2013).
23. Klaiman, S., Gromov, E. V. & Cederbaum, L. S. Extreme Correlation Effects in the Elusive Bound Spectrum of C_{60}^-. *J. Phys. Chem. Lett.* **4,** 3319–3324 (2013).
24. Voora, V. K. & Jordan, K. D. Nonvalence Correlation-Bound Anion State of C_6F_6: Doorway to Low-Energy Electron Capture. *J. Phys. Chem. A* **118,** 7201–7205 (2014).

25. Voora, V. K. & Jordan, K. D. Nonvalence Correlation-Bound Anion States of Polycyclic Aromatic Hydrocarbons. *J. Phys. Chem. Lett.* **6,** 3994–3997 (2015).
26. Gahl, C., Ishioka, K., Zhong, Q., Hotzel, A. & Wolf, M. Structure and dynamics of excited electronic states at the adsorbate/metal interface: C_6F_6/Cu(111). *Faraday Discuss.* **117,** 191–202 (2000).
27. Dougherty, D. B., Feng, M., Petek, H., Yates, J. T. & Zhao, J. Band Formation in a Molecular Quantum Well via 2D Superatom Orbital Interactions. *Phys. Rev. Lett.* **109,** 266802 (2012).
28. Field, D., Jones, N. C. & Ziesel, J.-P. Cold electron scattering in SF_6 and C_6F_6: Bound and virtual state channels. *Phys. Rev. A* **69,** 052716 (2004).
29. Suess, L., Parthasarathy, R. & Dunning, F. B. Nondissociative low-energy electron attachment to SF_6, C_6F_6, $C_{10}F_8$, and c-C_7F_{14}: Negative ion lifetimes. *J. Chem. Phys.* **117,** 11222–11227 (2002).
30. Dessent, C. E. H., Kim, J. & Johnson, M. A. Photochemistry of Halide Ion−Molecule Clusters: Dipole-Bound Excited States and the Case for Asymmetric Solvation. *Acc. Chem. Res.* **31,** 527–534 (1998).
31. Lehr, L., Zanni, M. T., Frischkorn, C., Weinkauf, R. & Neumark, D. M. Electron Solvation in Finite Systems: Femtosecond Dynamics of Iodide·$(Water)_n$ Anion Clusters. *Science* **284,** 635–638 (1999).
32. Lecointre, J., Roberts, G. M., Horke, D. A. & Verlet, J. R. R. Ultrafast Relaxation Dynamics Observed Through Time-Resolved Photoelectron Angular Distributions. *J. Phys. Chem. A* **114,** 11216–11224 (2010).
33. Stolow, A., Bragg, A. E. & Neumark, D. M. Femtosecond Time-Resolved Photoelectron Spectroscopy. *Chem. Rev.* **104,** 1719–1758 (2004).
34. Bailey, C. G., Dessent, C. E. H., Johnson, M. A. & Bowen, K. H. Vibronic effects in the photon energy-dependent photoelectron spectra of the CH3CN$^-$ dipole-bound anion. *J. Chem. Phys.* **104,** 6976–6983 (1996).
35. Steele, D. & Whiffen, D. H. The vibrational frequencies of hexafluorobenzene. *Trans. Faraday Soc.* **55,** 369–376 (1959).
36. Jordan, K. D. private communication.

37. Mbaiwa, F., Van Duzor, M., Wei, J. & Mabbs, R. Direct and Indirect Detachment in the Iodide−Pyrrole Cluster Anion: The Role of Dipole Bound and Neutral Cluster States. *J. Phys. Chem. A* **114,** 1539–1547 (2010).

38. King, S. B. *et al.* Electron accommodation dynamics in the DNA base thymine. *J. Chem. Phys.* **143,** 024312 (2015).

39. Miller, T. M., Van Doren, J. M. & Viggiano, A. A. Electron attachment and detachment: C_6F_6. *Int. J. Mass Spectrom.* **233,** 67–73 (2004).

40. Nakajima, A. *et al.* Photoelectron spectroscopy of $(C_6F_6)^-_n$ and $(Au\text{-}C_6F_6)^-$ clusters. *Chem. Phys. Lett.* **214,** 22–26 (1993).

41. Eustis, S. N., Wang, D., Bowen, K. H. & Naresh Patwari, G. Photoelectron spectroscopy of hydrated hexafluorobenzene anions. *J. Chem. Phys.* **127,** 114312 (2007).

42. Mbaiwa, F., Wei, J., Van Duzor, M. & Mabbs, R. Threshold effects in $I^-\cdot CH_3CN$ and $I^-\cdot H_2O$ cluster anion detachment: The angular distribution as an indicator of electronic autodetachment. *J. Chem. Phys.* **132,** 134304 (2010).

43. Mbaiwa, F., Dao, D., Holtgrewe, N., Lasinski, J. & Mabbs, R. Inter-channel effects in monosolvated atomic iodide cluster anion detachment: Correlation of the anisotropy parameter with solvent dipole moment. *J. Chem. Phys.* **136,** 114303 (2012).

44. Weber, J. M., Leber, E., Ruf, M.-W. & Hotop, H. Nuclear-Excited Feshbach Resonances in Electron Attachment to Molecular Clusters. *Phys. Rev. Lett.* **82,** 516–519 (1999).

45. Dessent, C. E. H., Bailey, C. G. & Johnson, M. A. On the vibrational fine structure in the near-threshold photofragmentation spectrum of the $I^-\cdot CH_3I$ complex: Spectroscopic observation of nonadiabatic effects in electron-molecule scattering. *J. Chem. Phys.* **105,** 10416–10423 (1996).

46. Roberts, G. M., Nixon, J. L., Lecointre, J., Wrede, E. & Verlet, J. R. R. Toward real-time charged-particle image reconstruction using polar onion-peeling. *Rev. Sci. Instrum.* **80,** 053104 (2009).

47. Shao, Y. *et al.* Advances in molecular quantum chemistry contained in the Q-Chem 4 program package. *Mol. Phys.* **113,** 184–215 (2015).

48. Yanai, T., Tew, D. P. & Handy, N. C. A new hybrid exchange–correlation functional using the Coulomb-attenuating method (CAM-B3LYP). *Chem. Phys. Lett.* **393,** 51–57 (2004).
49. Dunning, T. H. Gaussian basis sets for use in correlated molecular calculations. I. The atoms boron through neon and hydrogen. *J. Chem. Phys.* **90,** 1007–1023 (1989).
50. Peach, M. J. G., Tellgren, E. I., Sałek, P., Helgaker, T. & Tozer, D. J. Structural and Electronic Properties of Polyacetylene and Polyyne from Hybrid and Coulomb-Attenuated Density Functionals. *J. Phys. Chem. A* **111,** 11930–11935 (2007).
51. Cohen, A. J., Mori-Sánchez, P. & Yang, W. Insights into Current Limitations of Density Functional Theory. *Science* **321,** 792–794 (2008).
52. Sherrill, C. D. Frontiers in electronic structure theory. *J. Chem. Phys.* **132,** 110902 (2010).
53. Peterson, K. A., Shepler, B. C., Figgen, D. & Stoll, H. On the Spectroscopic and Thermochemical Properties of ClO, BrO, IO, and Their Anions. *J. Phys. Chem. A* **110,** 13877–13883 (2006).

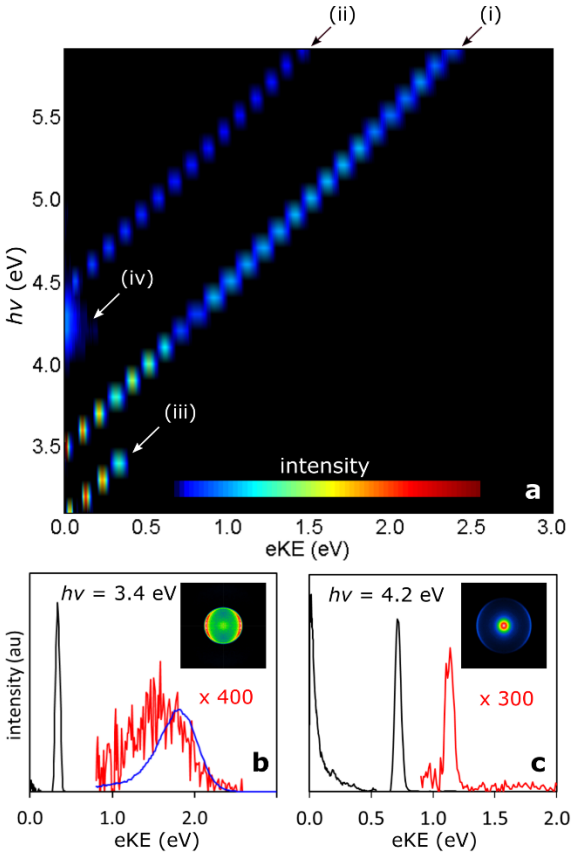

Figure 1: Photoelectron spectra of $I^-\cdot C_6F_6$. a: Frequency resolved photoelectron spectra normalised to total signal. Features (i) and (ii) correspond to direct photodetachmnent leaving the neutral iodine in its $^2P_{3/2}$ or $^2P_{1/2}$ states, respectively. Feature (iii) corresponds to detachment from unclustered I^-. Feature (iv) corresponds to delayed autodetachment from an excited state accessed around 4.2 eV. **b**: Photoelectron spectra at $h\nu$ = 3.4 eV with the raw photoelectron image inset. For eKE > 0.8 eV, the intensity has been scaled to show detachment from $I\cdot C_6F_6^-$ (red) with the photoelectron spectrum of $C_6F_6^-$ (blue) shown for comparison. **c**: Photoelectron spectrum taken at $h\nu$ = 4.2 eV, with the raw photoelectron image inset, showing low eKE signal and a peak corresponding to feature (i) in **a**. Signal at eKE > 0.8 eV has been scaled (red) to highlight photodetachment from unclustered I^-. The polarisation axes for both raw photoelectron images is vertical.

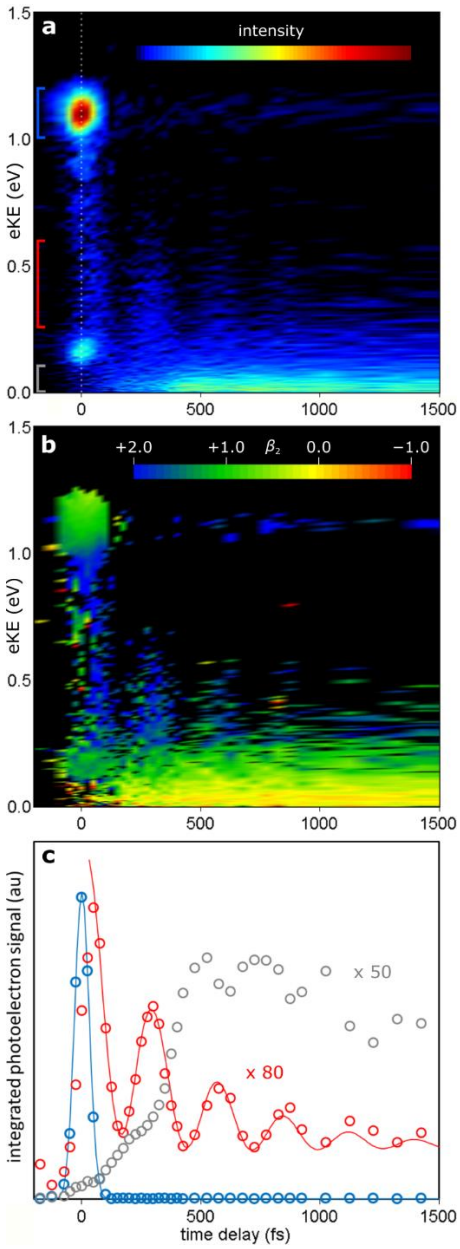

Figure 2: Time-resolved dynamics of $I^-\cdot C_6F_6$ following excitation at 3.10 eV. a: Time-resolved photoelectron spectra of $I^-\cdot(C_6F_6)$ with t =0 indicated by vertical dashed line. **b**: Time-resolved anisotropy parameters associated with **a** (blacked out regions have photoelectron signal <4% of maximum in **a**). **c**: Integrated photoelectron signal (open circles) over spectral windows indicated by correspondingly coloured square brackets in **a**. The red and grey widows have been scaled for clarity. Fits to the dynamics are shown in solid lines.

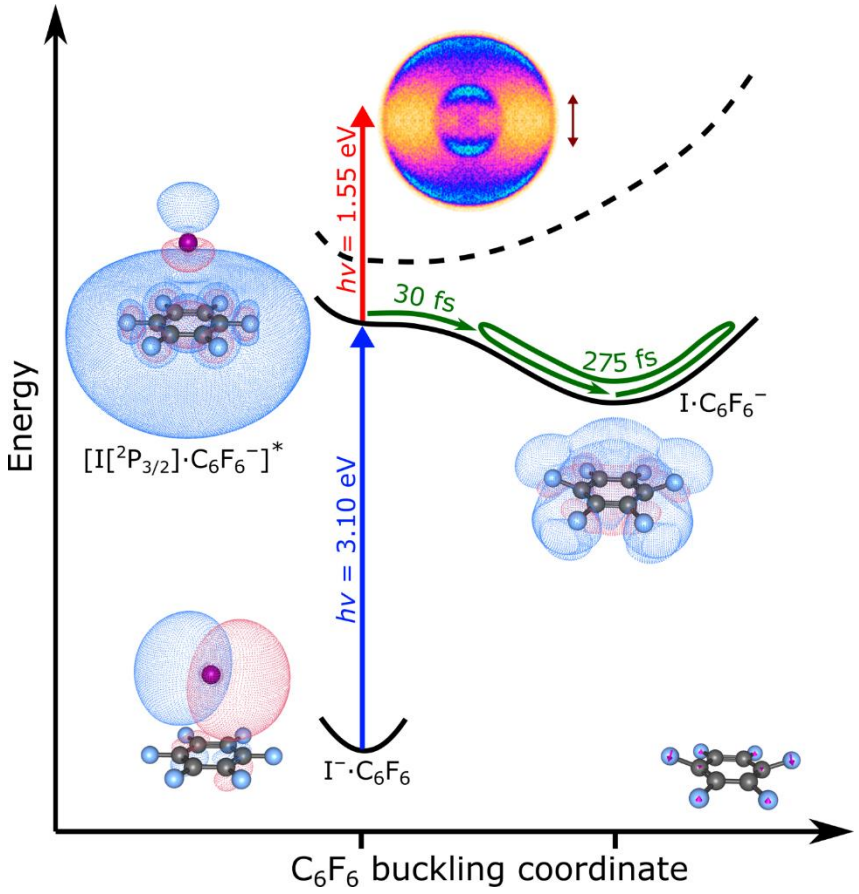

Figure 3: Schematic energy level diagram and molecular orbitals involved in electron capture. The coordinate represents the buckling mode of the C_6F_6 molecule shown. The initial $I^-\cdot C_6F_6$ is photoexcited (vertical blue arrow) from a 5p orbital localised on I^- to a charge transfer state, which is similar in character and shape to the correlation-bound state of $C_6F_6^-$. Photodetachment (vertical red arrow) from this diffuse orbital produces a highly anisotropic photoelectron image as shown (polarisation axes of pump and probe shown as adjacent double arrow). Evolution of this state along the buckling coordinate leads to a valence-bound state of $C_6F_6^-$ with a concomitant increase in the energy of the neutral surface, depicted by the dashed line. The increase in the energy gap leads to a smaller Franck-Condon window accessible by the probe leading to fewer observable photoelectrons.